Proceedings of the Twenty-sixth (2016) International Ocean and Polar Engineering Conference **www.isope.org**
Rhodes, Greece, June 26-July 1, 2016

ISBN 978-1-880653-88-3; ISSN 1098-6189

Numerical Simulation of Ship-Ship Interactions in Shallow Water

Qingjie Meng, Decheng Wan, Gang Chen*

State Key Laboratory of Ocean Engineering, School of Naval Architecture, Ocean and Civil Engineering, Shanghai Jiao Tong University, Collaborative Innovation Center for Advanced Ship and Deep-Sea Exploration, Shanghai, China
*Corresponding author

ABSTRACT

The objective of this study is to predict and analyze the viscous flow and the ship-ship interaction between two different tankers KVLCC2 and Aframax advancing in shallow water with same speed and with a fixed separation distance by solving the unsteady RANS equations in combination with the k-ω SST turbulence model. The computational results of the resistance, lateral force, yawing moment, as well as wave height measured by the wave gauge are validated against EFD conducted in Flanders Hydraulics Research (FHR) towing tank. Though the error for case A is not so satisfactory by up to 73%EFD, the tendency is agreed well with EFD data. Moreover, the error case B is much batter by less than 6.25% for both ships. For better understanding of the ship-ship interactions, the wave pattern of the free surface, surface pressure distribution of the ship hull, the asymmetric ship wake and vortex system are also given.

KEY WORDS: ship-ship interaction; shallow water; viscous flow;

INTRODUCTION

With the birth of the very large crude carriers (VLCC) and ultra large crude carriers (ULCC), which have been proven to be one of the best solution to satisfy the demands of oil transportation, a new problem arose. Many ports, which may not be deep enough or have narrow entrances or small births, are not suited to receive ships of such big seizes. On the other hand, a commercial ship which is not under navigating is just a very expensive warehouse. Therefore, the time spent in the harbor, which is mainly determined by the time needed to unload and re-load the oil, must be as short as possible. Both the two problems can be solved by the lightering operation. However, manoeuvring such large vessels without the assistance of tugs at a precision of meters is highly difficult. On top of these difficulties, hydrodynamic interaction forces take place, which influence greatly the relative motion of the vessels. This can result in accidents with important consequences as oil spills or severe damage to the vessels.

In order to perform lightering operation safely the understanding of the interaction effects between both ships is crucial. The ship-ship interactions is extremely complex and multiple parameters influence the final outcome (De Decker, 2006). Several methods are used in order to examine of the ship-ship interactions. Real scale and model scale tests can be carried out, but reliable simulations are necessary to examine the mechanism in an affordable and efficient manner.

Silverstein (1957) studied the lateral force and the yawing moment caused by the ship-ship interaction with linearized theory. Lataire et al. (2009) conducted a captive model test program for the ship lightering operation to provide the knowledge of the ship performance. The tests were also contributed as benchmark tests to the Second International Conference on Ship Manoeuvring in Shallow and Confined Water (2011), and the experimental data was also made available for CFD validation. Skejic and Berg (2009, 2010) used a unified seakeeping and manoeuvring theory to analyze the ship behavior during lightering operation in both clam water and waves. Xiang et al. (2011) studied the hydrodynamic interaction loads between two tankers during lightering operation in calm and deep water by utilizing a three dimensional potential flow method. Sadat-Hosseini et al. (2011) simulated the ship-ship interaction during lightering operation with RANS method and the results are compared with the experimental data. Lu et al. (2013) carried out a numerical study with SHIPFLOW to investigate the ship-to-ship interaction during a lightering operation. However, the free surface was neglected.

The objective of this study is to investigate the viscous flow and the interaction hydrodynamic forces and moment of two different tankers KVLCC2 and Aframax during lightering operation using URANS simulation. The tankers were advancing in shallow water with same speed and with a fixed separation distance. The capability of the present method for the prediction of the ship-ship interaction was confirmed by the good agreement of the predicted results with the corresponding experimental data, conducted in Flanders Hydraulics Research (FHR) towing tank. The wave pattern of the free surface, surface pressure distribution of the ship hull, the asymmetric ship wake as well as the vortex system were also predicted and analyzed to explain the ship-ship interaction.

CFD METHOD

The computation is carried out by an in-house code, which have been

discussed, applied, verified and validated for ship flows and have been proved to be competent in simulating the unsteady viscous flow around ships (Meng et al. 2013; 2014a; 2014b; 2015a; 2015b). The code is an overset, block structured URANS solver and was designed for ship applications using either absolute or relative inertial curvilinear coordinate system for arbitrary moving but non-deforming control volumes. The blended k-ε / k-ω turbulence model (Menter, 1994) was utilized. The free surface was captured by using single-phase level set method (Osher, et al., 1988; Sussman, et al., 1974). Numerical methods include higher order finite differences, PISO algorithm (Issa, 1986) for pressure-velocity coupling and parallelization with MPI-based domain decomposition. The computational domain was discretized using multi-block and dynamic overset structured grids, which was achieved by SUGGAR++ (Noack, et al., 2009). Captive, part-captive and full 6DOF capabilities for multi-objects with parent/child hierarchy are consequently available.

SIMULATION DESIGN

Ships introduction

The problem under study is the viscous flow around two tankers KVLCC2 and Aframax advancing in shallow water with same speed and with a fixed separation distance. KVLCC2 (the second variant of the KRISO Very Large Crude-oil Carrier) is extensively used in ship hydrodynamic investigation, as it is one of the benchmark models adopted by ITTC, SIMMAN Workshops, et al. Aframax tanker was originated from the Average Freight Rate Assessment tanker rate system. The Aframax tanker was widely used in industry but not yet much in CFD applications. 1/75 model scale ship models were used in the simulation. The body plan and hull geometry of both ships are respectively exhibited in Figs. 1-2, and the model-scale hull data are listed in Tables 1.

Table 1 Principal dimensions of the ship models

			Aframax	KVLCC2
Ship length		L_{pp} (m)	3.085	4.267
Beam		B (m)	0.56	0.773
Draft	T_F/T_A (m)	Design condition	0.2/0.2	
		Ballast condition	0.1/0.121	
	T_F/T_A (m)	Design condition		0.277/0.277
		loading condition		0.171/0.171

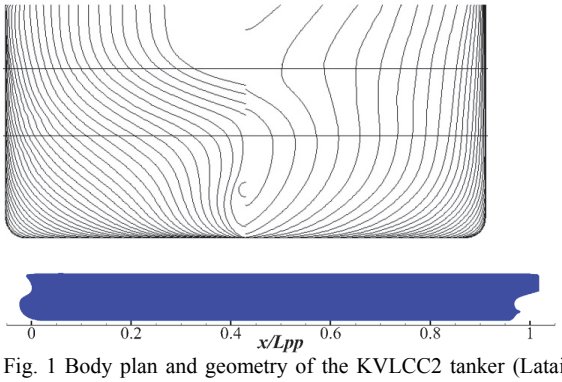

Fig. 1 Body plan and geometry of the KVLCC2 tanker (Lataire et al., 2009)

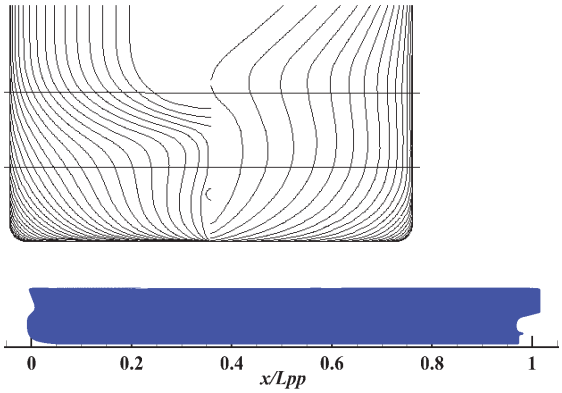

Fig. 2 Body plan and geometry of the Aframax tanker (Lataire et al., 2010)

Case Conditions

Two cases are presented in this paper. The Aframax tanker model was chosen as the reference hull. The KVLCC2 model was fixed at 1.007 m from the center of the towing tank. Three wave gauges was mounted in the towing tank to measure the wave height. An illustration of the test setting is given in Fig. 3 and details of the case conditions are shown in table 2.

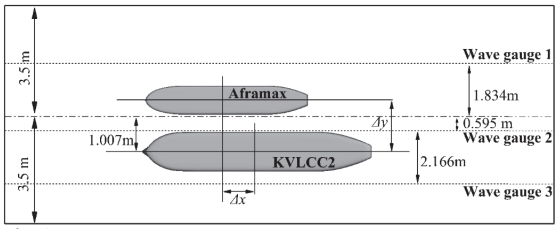

Fig. 3. Test setup.

Table 2 Details of the case conditions

	Aframax/KVLCC2		
		A	B
Water depth	h (m)	0.230	0.475
Draught	$T_{aframax}$	0.100	0.100
	T_{KVLCC2}	0.171	0.277
Ship speed	U (m/s)	0.356	0.356
Froude number	F_r	0.065	0.065
Froude number based on water depth	F_h	0.237	0.165
Reynolds number	Re ($\times 10^{-6}$)	1.094	1.094
Longitudinal position	Δx	1.543	0
Transverse position	Δy	1.3335	0.9995

Computational Domain, Coordinate System and Boundary Conditions

Considering the asymmetry of the flow field, the computational domain was set to cover two hulls. Taking case A as example, a schematic diagram indicating the coordinate system and the computational domain is displayed in Fig. 4. The computational domain extends within $-2.0 \leq x \leq 3.5$, $-1.135 \leq y \leq 1.135$ for both cases, and $-0.0746 \leq z \leq 0.25$ for case A, $-0.154 \leq z \leq 0.25$ for case B. A right-handed Cartesian coordinate system is fixed on the Aframax ship model with its origin located at the intersection of the water plane, the ship center-plane and the mid-ship section. The longitudinal Ox-axis is along the inflow, the

Oz-axis is vertical and points upward, and the undisturbed free surface is taken as the plane $z = 0$. For later comparison of the numerical results with the experimental data, the realistic boundary conditions is defined with reference to test conditions. The computational domain is made up of six kinds of boundaries. Inlet boundary condition is used for the upstream of background, while Exit condition is applied for the downstream of background. No-slip wall conditions are utilized on the solid hull surface. An impermeable slip boundary conditions condition is required on the bottom of the background. The far-field boundary conditions are specified on the top of the background. On the other hand, note that the ratio of both ship beams to towing tank width is about 10% and both are located about the middle of tank so that the effects of walls should be negligible in the experiment. So, in order to speed up the numerical convergence, zero gradient boundary condition is applied on the two sides of background.

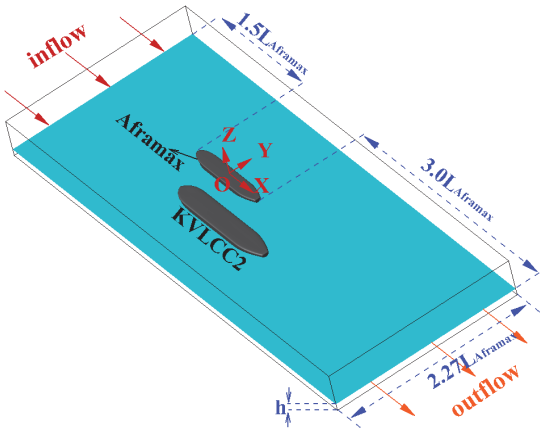

Fig. 4 Coordinate system and computational domain

Grid Design

For all cases, structured grids are used and overset gird technique is utilized to reduce the difficulty of the generation of structured grids in shallow water. The grid systems consists of a background orthogonal grid, which mimics the towing tank, and two boundary layer curvilinear grid which conform to the ships geometry where two clusters of grid points are concentrated around the bow and stern regions. A sketch of the grid distribution is shown in Figs. 5-7. Since no wall function is used in this study, the minimum size of the grid cell is refined to 10^{-6} on the boundary layer area to satisfying the condition $y+ < 1$ and to capture the detailed fluid property due to the turbulence. All the grids are refined in the vertical direction in $-0.002 \leq z \leq 0.002$, where the free surface is expected. Fig. 8 shows the overset grid systems of two ships and background. The total number of the grid points is about 6.05 million. The grids are summarized in Table 3.

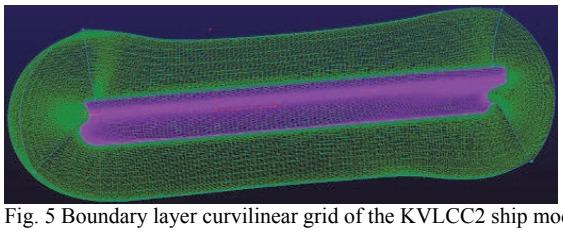
Fig. 5 Boundary layer curvilinear grid of the KVLCC2 ship model

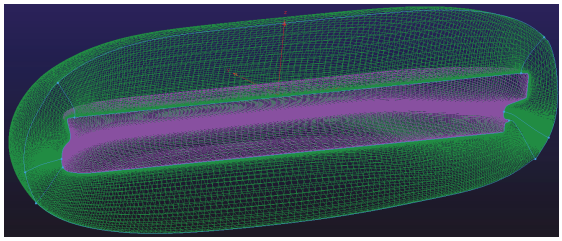
Fig. 6 Boundary layer curvilinear grid of the Aframax ship model

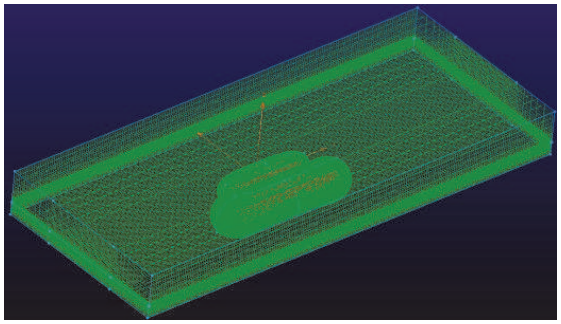
Fig. 7 A sketch of the grid distribution

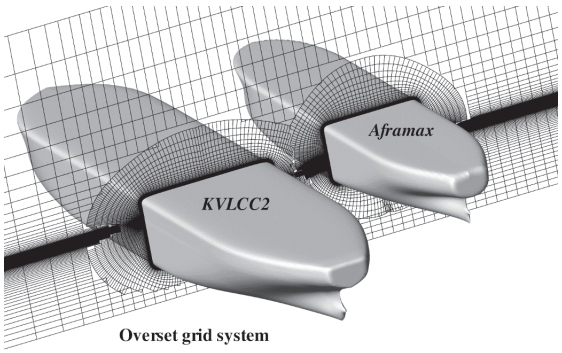

Fig. 8 A sketch of the overset grid systems

Table 3 Summary of the grids used in this study

	Grid number
Boundary layer grids of half of the KVLCC2 hull	169×48×131
Boundary layer grids of half of the Aframax hull	151×48×141
Background	201×141×71
Total	6,047,872

RESULTS AND ANALYSIS

Hydrodynamic Forces and moment

The comparison of the computational results of resistance *X*, lateral force *Y*, and yawing moment *N* and experimental data is shown in Table 4. The results are presented in EFD ship-fixed right-handed coordinate system in which *x* pointing to the upstream, and *z* pointing downward and the free-surface at rest lies at $z = 0$.

In case A, resistance of Aframax is predicted by 73%EFD, the lateral force has error of -3.0%EFD, and the error of yawing moment is -16%. For the KVLCC2, the error of resistance, lateral force, and yawing moment is 30%EFD, -30%EFD and -22%, respectively. The

disagreement might result from the extremely complex flow influenced by the shallow water. The flow field will be analyzed later to reveal the sources of the differences. In case B, a very good agreement was obtained for X, Y, N with 1.9%EFD, 1.0%EFD, 3.5%EFD for Aframax and -6.25%EFD, 4.9%EFD, 1.1%EFD for KVLCC2. The better results of case B indicate that the computational accuracy increases with increasing water depth. In both cases, the negative lateral force on Aframax and positive one on KVLCC2 demonstrate an attraction force between the ships. The larger longitudinal distance of case A might lead to the smaller attraction force between the ships than that of case B.

Table 4 Comparison of steady integral variables with experimental data

			R (N)	Y (N)	N (Nm)
Case A	Aframax	EFD	-0.97	-0.30	1.38
		CFD	-1.68	-0.29	1.15
		E(%)	73	-3.0	-16
	KVLCC2	EFD	-0.96	0.85	3.44
		CFD	-1.25	1.10	2.68
		E(%)	30	-30.0	-22
Case B	Aframax	EFD	-0.68	-1.150	0.11
		CFD	-0.69	-1.152	0.114
		E(%)	1.9	1.0	3.5
	KVLCC2	EFD	-2.37	0.85	-0.74
		CFD	-2.22	0.89	-0.75
		E(%)	-6.25	4.9	1.1

Wave pattern and wave height

For better understudying the ship-ship interactions during lightering and to find the sources of the large error of case A, the wave pattern and wave height was predicted and analyzed.

Fig. 9-10 present the wave pattern of case A and case B, respectively. The Froude number based on water depth F_h is far less than 1.0 for both cases. In other words, ships are at subcritical speed and ship speed is slower than the phase speed of waves. As a result, the diverging wave is dominant and no transverse waves and Kelvin envelope is shown. This is the characteristic of the solitary wave in shallow water and successfully captured by the URANS simulation. The diverging waves, shown in Figs. 9-10, transmit to the two sides with the angle around 180 degrees. On the other hand, the lowest wave trough is located between two ships and the depth of wave trough increases as being close to the ships. This conclusion is further supported by the result in Fig. 11.

Fig. 11 presents the wave height detected in the three locations where the three gauges are placed in the experiment. Three gauges are located at y = -1.834 m, y = 0.595 m, and y = 2.166 m, respectively. The wave crest for bow and stern wave of gauge2 are predicted well, but the results of wave trough of gauge2 are a bit over predicted. As a result, the pressure resistance will be over predicated and the predicted resistance of both ships is also amplified. As shown in Fig. 3, the gauge2 locates between the two ships. So, it detects the lowest wave trough due to the lower pressure caused by narrower channel between two ships. The gauge3 obtains the lower wave trough than the gauge1 does because it is closer to the ship. The CFD result also presents this kind of trend but has some error. As discussed above, the effects of walls was negligible in the simulation by apply zero gradient boundary condition on the two sides of background. The error might be caused by the wall effect, such as the wave reflection or the channel between ships and side walls of the towing tank.

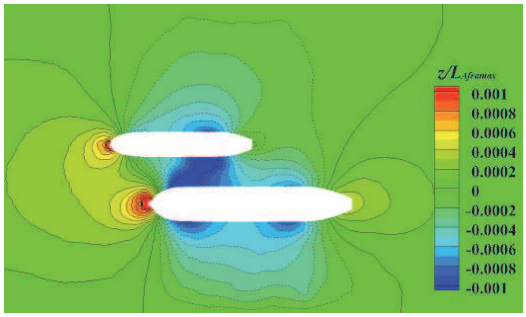

Fig. 9 Wave pattern of case A

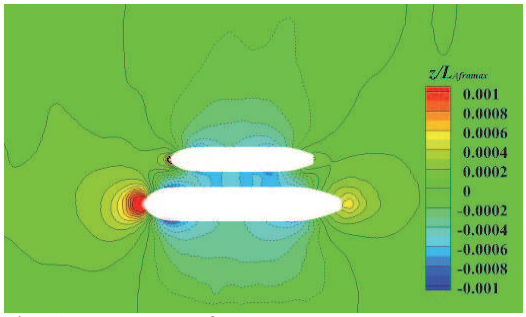

Fig. 10 Wave pattern of case B

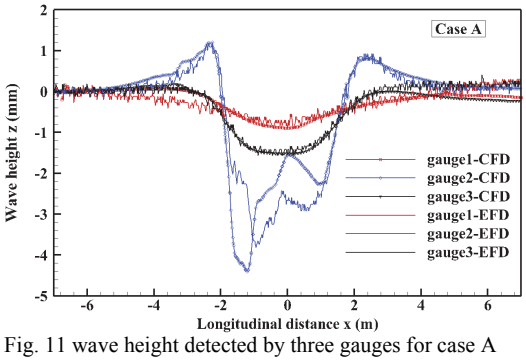

Fig. 11 wave height detected by three gauges for case A

Surface pressure distribution

Taken case A as example, the distribution of pressure coefficient on the ships explaining the negative Y on the Aframax and positive Y on the KVLCC2 in Table 4 is given in Fig. 12. The pressure distributions are represented by a nondimensionalized pressure coefficient called C_P, which is defined as:

$$C_P = \frac{P}{\frac{1}{2}\rho U^2}$$

where P denotes the pressure on the ship hull [N/m^2], ρ represents the density of water [Ns^2/m^4], and U is the reference velocity [m/s].

The low wave height due to the low pressure between two ships caused the decrease of the surface pressure. Then a strong suction generated between the stern of the Aframax and the bow of the KVLCC2 is noticed. Also, the suction force will generate a moment to starboard for both ships, which further support the result and discussions in Table 4.

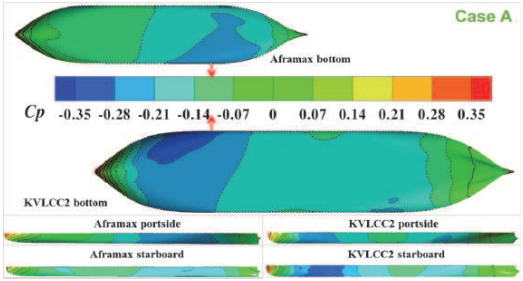

Fig. 12 Computational pressure distribution on the ships for case A

Wake and velocity distribution

The computational velocity distribution around both ships for case A and case B are presented in Figs. 13-14. Ships are very close to each other and the flow is forced between two ships, which causes the disturbed flow between ships and the rise of the velocity of the water particles between ships. Due to Bernoulli effect the pressure between ships will drop, which causes the interaction forces between ships. The thick boundary layer, huge low-speed areas and asymmetric ship wake are presented obviously on the portside of stern of the Aframax for case A and both side of stern of the KVLCC2 for both case A and case B. The low-speed areas around the stern of Aframax are not obvious for case B.

The water depth was defined as (PIANC, 1992):

Deep water	$h/T > 3.0$;
Medium deep water	$1.5 < h/T < 3.0$;
Shallow water	$1.2 < h/T < 1.5$;
Very shallow water	$h/T < 1.2$;

The effect of the water depth can be noticed in medium deep water, is very significant in shallow water, and dominates the ship's behavior in very shallow water (23rd ITTC, 2005). For KVLCC2, h/T_{KVLCC2} increases slightly from h/T_{KVLCC2}=1.345 to h/T_{KVLCC2}=1.715 for case A and case B. In other words, the water depth changes from shallow water to medium deep water for KVLCC2. As a result, the low-speed areas did not decrease much. However, the situation is different for Aframax. Comparing case A and case B, $h/T_{Aframax}$ increases from $h/T_{Aframax}$=2.3 to $h/T_{Aframax}$=4.75, which means the water depth for Aframax changes from medium deep water to deep water, where the effect of water depth cannot be noticed. So, the low-speed areas around the stern of Aframax is almost disappear.

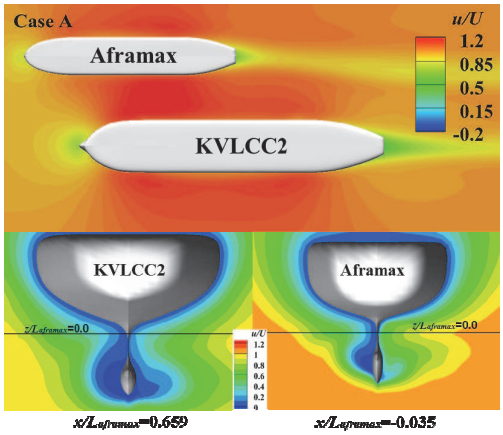

Fig. 13 Velocity distribution around the ships for case A

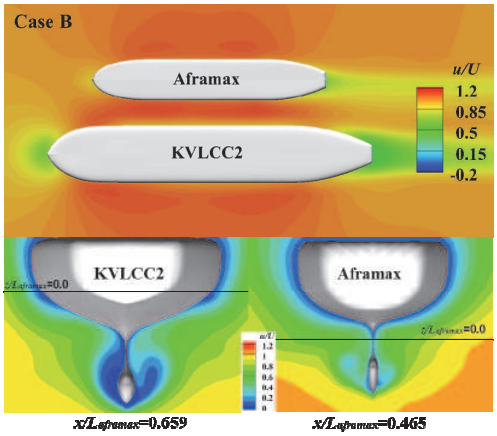

Fig. 14 Velocity distribution around the ships for case B

Vortex system

Fig. 15-16 shows the vortex system of both ships with velocity contour on the iso-surface of Q=20. Because of the low Froude number in both cases, the bow vortices on the two ships are not significant. The high-velocity area near the bow of KVLCC2 for case A is caused by the shallow water effect. Though the relative position of the two ships of case A is larger, due to the shallower water depth the vortices around the parallel middle body of case A are more significant than that of case B. But, the vortices system near the stern of case B shows more significant for both ships. This might be caused by the smaller longitudinal distance of two ships for case B. On the other hands, as the smaller lateral distance of two ships of case B, the vortices present the interaction effects.

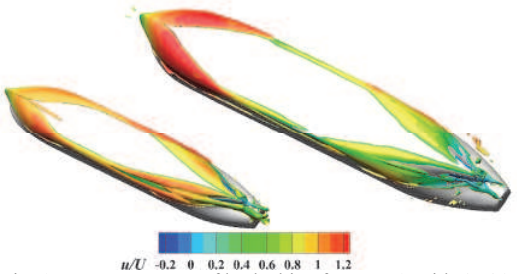

Fig. 15 Vortex system of both ships for case A with Q=20

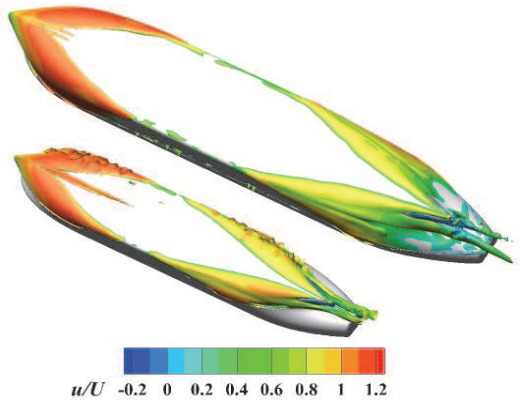

Fig. 16 Vortex system of both ships for case B with Q=20

CONCLUSIONS AND FUTURE WORK

The ship-ship interaction between two tankers KVLCC2 and Aframax during lightering operation in shallow water was investigated and reported numerically. The computational results of resistance, lateral force, yawing moment, as well as wave height were validated against EFD conducted in FHR towing tank. The results of case B show fairly good agreement with the experimental data. Results of case A qualitatively agree well with EFD data, with nonnegligible error, which might could be improved by considering the wall effect and improved grids. The results confirm the capability of the present method for the prediction of the viscous flow around the ships during lightering operation. With the advantages of CFD method, more details of the flow field was also computed and presented to explain the hydrodynamic performance of the ships during lightering operation in shallow water. And the simulations reveal several influences of the ship-ship interactions such as the suction forces and asymmetric ship wakes, as well as the solitary wave in shallow water.

In the future work, more cases will be simulated to study the effects of longitudinal position, transverse position, and water depth on the flow field surrounding both ships.

ACKNOWLEDGEMENTS

This work is supported by the National Natural Science Foundation of China (51379125, 51490675, 11432009, 51579145, 11272120), Chang Jiang Scholars Program (T2014099), Program for Professor of Special Appointment (Eastern Scholar) at Shanghai Institutions of Higher Learning (2013022), Innovative Special Project of Numerical Tank of Ministry of Industry and Information Technology of China (2016-23) and Foundation of State Ley Laboratory of Ocean Engineering (GKZD010065), to which the authors are most grateful.

REFERENCES

27th International Towing Tank Conference, (2014), available at: http://ittc.info/, Copenhagen, Denmark.

De Decker, B (2006). "Ship–Ship Interaction during Lightering Operations," Doctoral dissertation, Ghent University.

Issa, R, (1986) "Solution of the implicitly discretized fluid flow equations by operator-splitting", Journal of computational physics, 62 (1): 40-65.

ITTC, the Manoeuvring Committee, (2005). "Final Report and Recommendations to the 24th ITTC," *Proceeding of the 24th ITTC*.

Lataire, E, Vantorre, M, and Delefortrie, G (2009). "Captive model testing for ship-to-ship operations", *Proceedings of MARSIM2009*, Panama City, Panama.

Meng, QJ, Wan, DC (2013). "Numerical simulation of the viscous flow surrounding a ship with overset grid technique (in Chinese)," *Proceedings of the 13th national conference on hydrodynamics*, Qingdao, China, August 22-27, 1368-1373.

Meng, QJ, Wan, DC (2014a). "Numerical Simulations of Ship Motions in Confined Water by Overset Grids Method," *Proceedings of the 24th International Ocean and Polar Engineering Conference*. Busan, Korea, June 15-20, 463-469.

Meng, QJ, Wan, DC, (2014b). "Numerical predictions of the viscous flow around KVLCC2 in pure sway motion (in Chinese)," *Proceedings of the ship and ocean engineering CFD workshop*, Dalian, China, July 25-27, 184-190.

Meng, QJ, Wan, DC, Huang WH (2015a). "Numerical Investigation of Influence of Eccentricity on the Hydrodynamics of a Ship Maneuvering into a Lock", *Proceedings of the 6th International Conference on Computational Methods*, Auckland, New Zealand, July 14-17, 2015

Meng, QJ, Wan, DC (2015b). "Numerical Simulations of Viscous Flows around a Ship While Entering a Lock With Overset Grid Technique", *Proceedings of the 25th International Ocean and Polar Engineering Conference*, Kona, Hawaii, USA, June 21-26, 2015: 989-996.

Menter, FR, (1994) "Two-Equation Eddy Viscosity Turbulence Models for Engineering Applications", *AIAA Journal*, Vol. 32(8):1598-1605.

Noack, RW, Boger, DA, Kunz, RF, Carrica, PM, (2009) "Suggar++: An Improved General Overset Grid Assembly Capability", *Proceedings of the 19th AIAA Computational Fluid Dynamics Conference*, San Antonio, Texas, USA, AIAA 2009-3992.

Osher, S, and Sethian, JA, (1988) "Fronts propagating with curvature-dependent speed: algorithms based on Hamilton-Jacobi formulations", *Journal of computational physics*, 79(1), 12-49.

PIANC, (1992). "Overview of simulation techniques, capability ship maneuvering simulation models for approach channels and fairway in harbours".

Sadat-Hosseini, H, Wu, PC, Toda, Y, Carrica, P, and Stern, F (2011). "URANS studies of ship–ship interactions in shallow-water". *Proceedings of the Second International Conference on Ship Manoeuvring in Shallow and Confined Water*, Trondheim, Norway.

Second International Conference on Ship Manoeuvring in Shallow and Confined Water: Ship-to-Ship Interaction, Trondheim, Norway, 2011 (http://www.shallowwater.ugent.be/EN/kc_conf_sts_EN.htm).

Silverstein, BL (1957). "Linearized theory of the interaction of ships", Doctoral dissertation, Univ. of California.

SIMMAN2014, (2014) available at: http://simman2014.dk/, Lyngby, Denmark.

Skejic, R, Berg, TE, (2009). "Hydrodynamic interaction effects during lightering operation in calm water – theoretical aspects", *Proceedings of the International Conference on Marine Simulations and Ship Manoeuvability – MARSIM 2009*, Panama City, Panama.

Skejic, R, Berg, TE, (2010). "Combined seakeeping and manoeuvring analysis of a two-ship lightering operations", *Proceedings of the ASME 2010 29th International Conference on Ocean, Offshore and Arctic Engineering, OMAE2010*, Shanghai, China.

Sussman, M, Smereka, P, Osher, S, (1994) "A level set approach for computing solutions to incompressible two-phase flow", *Journal of Computational Physics*, 114 (1): 146-159.

Xiang, X, Skejic, R, Faltinsen, OM, and Berg, TE (2011). "Hydrodynamic interaction loads between two ships during lightering operation in calm water", *Proceedings of the 2nd International Conference on Ship Manoeuvring in Shallow and Confined Water*, Trondheim, Norway.

Zou, L, Larsson, L, (2013). "Numerical predictions of ship-to-ship interaction in shallow water", *Ocean Engineering*, 72, 386-402.